International Journal of Heat and Mass Transfer 183 (2022) 122098

Contents lists available at ScienceDirect

International Journal of Heat and Mass Transfer

journal homepage: www.elsevier.com/locate/hmt

In-situ thermal conductivity of a sorption composite: An analytical approach

A. Shafiepour, C. McCague, M. Bahrami*

Laboratory for Alternative Energy Conversion (LAEC), School of Mechatronic Systems Engineering, Simon Fraser University, BC V3T 0A3, Canada

ARTICLE INFO

Article history:
Received 18 May 2021
Revised 25 September 2021
Accepted 11 October 2021
Available online 27 October 2021

Keywords:
Functional composites
Sorption system
Heat and mass transfer
Thermal conductivity
Natural graphite
Thermal diffusivity
Analytical modeling

ABSTRACT

This paper presents a new analytical quasi-steady-state model to estimate the effective thermal conductivity and thermal diffusivity of wetted sorbent composites containing thermally-conductive additives which is developed based on the effective medium theory, or unit cell approach, and covers all salient morphological parameters, material properties, and operating conditions. The proposed closed-form solution is validated with experimental data using several consolidated salt-in-matrix sorbents with silica gel, $CaCl_2$, polyvinyl alcohol (PVA) binder, and 0–15 wt.% of graphite flakes (GF), as well as 0–5 wt.% of expanded natural graphite (ENG) as thermally-conductive additives fabricated and characterized in our lab. The addition of 15 wt.% of GF, and 5 wt.% of ENG to the sorbent composite when tested with a relative humidity (RH) of 2%, resulted in 536%, and 572% enhancement in the effective thermal conductivity. Also, increasing the sorbed water content in the composite with no thermally-conductive additives from 0.02 to 0.9 $g{\cdot}g^{-1}$ caused 318% increase in the thermal conductivity.

1. Introduction

The global cooling energy demand is projected to triple by 2050, which takes account of the likely effect of current policies and targets, with nearly 70% of the increase coming from the residential sector [1]. Meanwhile, countries accounting for more than 60% of global energy-related carbon emissions aim to bring their emissions down to net zero by 2050 or soon after [2]. As more than 80% of residential building energy consumption is used for heating and cooling purposes, there is a rising interest in efficient and sustainable heating, cooling, and thermal storage (heat transformer) systems that do not add more CO_2 to the environment [3]. One promising solution is heat-driven sorption technology. Sorption systems use benign environmentally friendly refrigerants, such as water, have no noise or vibration problems, and can generate cooling power from low-grade industrial waste heat or renewable thermal energy sources with temperatures below 90 °C, such as solar or geothermal heat [4].

High porosity sorbent materials-typically in the form of packed beds or consolidated composite coatings in sorption systems - often have low thermal conductivity and thermal diffusivity which impedes their heat transfer adversely affecting the overall performance. Low heat and mass transfer in sorbents result in low specific power (SP) which is one of the major limitations facing the commercialization of sorption heat transformer systems. Therefore, thermal conductivity of the consolidated sorbent layer is a fundamental property of the composite that can strongly affect the dynamic performance of sorption systems.

Several methods to enhance the heat transfer in sorption composites have been investigated. One common approach has been the addition of thermally conductive additives, which, when combined with the sorbent and binder, form higher conductivity paths to increase the overall thermal performance. The main challenge of this method is that the thermal conductivity of the composites can vary not only with composition, specifically the shape, and volume percentage of the additive, but also with the preparation conditions if they effect the overall density.

High thermal conductivity of graphite, along with the other above-mentioned benefits, made it the most studied additive for developing sorbent composite with the aim of improving thermal conductivity [5]. Mauran et al. [6], for example, reported the thermal conductivity of their $CaCl_2$-ENG sorbent composites to be 10–40 $W{\cdot}m^{-1}{\cdot}K^{-1}$. Wang et al. [7] measured the thermal conductivity for three types of sorbents namely, simple unconsolidated sorbent composite, consolidated sorbent composite with expanded graphite as additive, and pure $CaCl_2$ powder using the hot wire method. They reported that the thermal conductivity of the $CaCl_2$-expanded graphite consolidated sorbent composite to be in the range of 7.05–9.2 $W{\cdot}m^{-1}{\cdot}K^{-1}$ depending on the mass fraction of

Abbreviations: TPS, transient plane source; RH, relative humidity; ENG, expanded natural graphite; GF, graphite flakes; HEX, heat exchanger.

* Corresponding author.
E-mail address: mbahrami@sfu.ca (M. Bahrami).

https://doi.org/10.1016/j.ijheatmasstransfer.2021.122098
0017-9310/

Nomenclature

k	thermal conductivity, $W{\cdot}m^{-1}{\cdot}K^{-1}$
R	thermal resistance, $K{\cdot}W^{-1}$
T	temperature, K
$\dot{Q}$	heat flow rate, W
t	thickness, m
r	radius, m
L	unit cell length, m
u	uncertainty
d_p	pore size diameter, m
d_c	equivalent cubic diagonal, m
Greek	
α	thermal diffusivity, $m^2{\cdot}s^{-1}$
ω	water uptake, $g{\cdot}g^{-1}$
ε	porosity
ρ	density, $kg{\cdot}m^{-3}$
θ	angle, degree
φ	additive weight percentage
Subscripts	
eff	effective
m	medium
p	additive particle
s	solid host matrix
w	water

expanded graphite. Fayazmanesh et al. [8] studied the effect of adding graphite flakes as a thermally-conductive additive to a sorbent composite made of $CaCl_2$ in a silica gel matrix. The thermal conductivity of a set of sorbent composites made of silica gel B60, $CaCl_2$, and PVP40 with 0–15 wt.% of graphite flakes were measured at 2 and 20 RH% using a transient plane source (TPS) method. Their result indicates that the addition of 20 wt.% of graphite flakes increased the thermal conductivity of the sorbent composite from 0.57– 0.78 $W{\cdot}m^{-1}{\cdot}K^{-1}$. Eun et al. [9] investigated the effect of adding expanded graphite to sorbent composites made of silica gel. They also studied the effect of porosity on the sorbent thermal conductivity. Their results show the thermal conductivity of sorbent composites increased from 0.17 $W{\cdot}m^{-1}{\cdot}K^{-1}$ to a thermal conductivity range of 10–20 W $m^{-1}{\cdot}K^{-1}$ depending on the expanded graphite mass ratio in the composite. Zheng et al. [10] studied the effect of adding expanded natural graphite treated with sulfuric acid (ENG-TSA) to a silica gel sorbent composite to improve the thermal conductivity and adsorption performance of the composite. Their evaluation on non-equilibrium adsorption performance and equilibrium adsorption performance showed enhancement of both heat and mass transfer, respectively. They also reported that by adding ENG to the silica gel composite, they measured the maximum thermal conductivity of 19.1 $W{\cdot}m^{-1}{\cdot}K^{-1}$, which is 270 times higher than their pure silica gel composite.

During the sorption and desorption processes, the variation in sorbate (water) content can significantly affect the thermal conductivity and thermal diffusivity of consolidated sorption composites. For instance, Tanashev et al. showed that the thermal conductivity of $CaCl_2$/ mesoporous silica gel increased $\sim$ 285% from 0.13 to 0.5 $W{\cdot}m^{-1}{\cdot}K^{-1}$, as the absorbed water content increased from 0.1 to 0.8 $g{\cdot}g^{-1}$ [11]. Although, there is clear evidence of the dependence of thermal conductivity (k) on sorbent uptake, in the majority of available models of sorption systems, it is assumed to be a constant value [12–15]. Furthermore, there is no mechanistic model that can predict the thermal conductivity/diffusivity of such composites, as a function of pertinent morphological and operating conditions, during the de/sorption process.

A summary of published investigations of water uptake (ω) impact on the effective thermal conductivity of wetted porous medium and their studied parameters is presented in Table 1. The first study of the effect of water sorption on the thermal conductivity of a $SiO_2/CaCl_2$ system was carried out by Aristov et al. using a hot wire method [16,17]. They reported that thermal conductivity increased from 0.33 to 0.53 $W{\cdot}m^{-1}{\cdot}K^{-1}$ when the water uptake changed from 0.35 to 0.75 $g{\cdot}g^{-1}$. Freni et al. [18] measured the thermal conductivity of two sorbent composites made of silica gel with $CaCl_2$, or LiBr as salt, using a hot wire method under various conditions of vapor pressure (P_{wv}), temperature (T), and water uptake. They observed a 0.10 and 0.15 $W{\cdot}m^{-1}{\cdot}K^{-1}$ increase, respectively, in the thermal conductivity of their composites if the measurement ranges were chosen according to the operating conditions of a typical sorption cooling cycle (10 mbar $< P_{wv} <$ 70 mbar, 40 °C $< T <$ 130 °C).

Buonanno and Carotenuto [19] developed a model to predict a porous medium's effective thermal conductivity. Steady-state heat conduction in a two-phase system was studied using a volume averaging technique. Particle shape, roughness, and solid conductivity were also investigated. McGaughey and Kaviany [20] presented a molecular dynamic simulation-based analysis for thermal conductivity of a porous structure. The applied molecular dynamic simulation was rather sophisticated to be utilized in adsorption heat pump system simulations. Lu et al. [21] experimentally studied the effects of porosity, particle size, and natural convection on the effective thermal conductivity of a copper foam-air and copper foam-water system. A linear correlation to describe the contribution of fluid was proposed as a function of porosity and pore size. Dawoud et al. [22] developed a theoretical model for predicting the effective thermal conductivity of wetted zeolite. To validate their model, the effective thermal conductivity of 4A zeolite-water was measured by a transient hot wire method under various conditions of vapor pressure, temperature, and water loading representing a typical adsorption cooling cycle. However, various parameters were estimated by fitting the experimental data which limits the application of the model to a specific composite.

Tanashev and Aristov [23], measured the dependence of the thermal conductivity of the two-component sorbent $SiO_2/CaCl_2$ on the sorbed water uptake. They also measured the thermal conductivity of sorbents made of mesoporous silica gel and alumina with impregnated salt ($CaCl_2$, $MgCl_2$, and $LiBr_2$) [11]. For the three silica-based sorbents, similar dependencies of effective thermal conductivity as a function of uptake, $k(\omega)$, were found as: (i) a smooth rise at $\omega < \omega^* =$ 0.4–0.55, where ω^* is the uptake threshold (i.e., in this case, when the mesopores of silica gel are completely filled with the salt solution); and (ii) a sharp increase within the narrow uptake range near the threshold uptake ω^*. The transition occurs at the same fraction of the pore volume occupied by the salt solution regardless of the salt confined. Their obtained results were described by a heat transfer model in a porous wetted medium developed by Luikov et al. [24] and modified by Bjurstrm et al. [25]. Fayazmanesh et al. [8]. They studied the effect of water uptake on the effective thermal conductivity of the sorbent composite $SiO_2/CaCl_2$ and graphite flake as a thermally conductive additive. The thermal conductivity of a set of sorbent composites made of silica gel B60, $CaCl_2$, and PVP40 with 0–15 wt.% of graphite flakes were tested at 2 and 20 RH%. The increase in the absorbed water content from 0.06 to 0.19 $g{\cdot}g^{-1}$ was shown to increase the thermal conductivity of the sample from 0.3 to 0.48 $W{\cdot}m^{-1}{\cdot}K^{-1}$.

To the best of the authors' knowledge, no prior study investigated the effects of all salient parameters, including water uptake, porosity, and thermally conductive additives, simultaneously on the effective thermal conductivity of sorption composites. The absence of a mechanistic closed-form solution for the effective thermal conductivity of sorbent composites is noticeable.

Table 1
Summary of the existing studies on the effect of water uptake on the effective thermal conductivity of sorption composites.

Ref. No.	Sorbent/host matrix	Salt	Approach	Characteristics of the parametric study
[11, 23]	Silica gel alumina	$CaCl_2$ LiBr $MgCl_2$	Experimental	Water uptake salt material host matrix material
[22]	Zeolite 4A	–	Experimental theoretical model	Water uptake temperature
[18]	Silica gel	$CaCl_2$ LiBr	Experimental	Water uptake salt material temperature vapor pressure
[19]	–	–	Volume averaging model	Particle shape roughness solid conductivity
[20]	Silica zeolite-A	–	Molecular dynamic simulation	Water uptake
[25]	Silica gel	–	Analytical model experimental	Water uptake porosity temperature total gas pressure
[8]	Silica gel	$CaCl_2$	Experimental	Water uptake additive particle (Graphite flakes)
[21]	Copper foam	–	Experimental	Air and water uptake porosity natural convection

This study aims to fill this knowledge gap by developing a new 1-*D* quasi- steady-state analytical model for the effective thermal conductivity and diffusivity of a consolidated salt-in-matrix sorption composite. This methodology can be applied to other sorts of sorption composites as well. The model considers the key morphological and operational parameters, including thermal conductivity and density of silica, porosity, and pore size distribution of the host matrix, along with the thermal conductivity, density, aspect ratio, and size of the thermally conductive additive particles to determine the water uptake impact on the effective thermal conductivity of the composite during a sorption working cycle.

2. Experimental study

2.1. Sample preparation

Polyvinyl alcohol (PVA) binder (40,000 MW, Amresco Inc.) was dissolved in water; subsequently, $CaCl_2$ (Calcium chloride C77–500, 4–20 mesh, anhydrous, Fisher scientific), and silica gel (SiliaFlash® B150, Silicycle, Inc., Quebec, Canada) and different amount of graphite flakes (808,091, 99% Carbon, + 100 mesh), consisting of both 150 μm fine particles and thin flakes up to 1.3 mm long, Sigma-Aldrich, or expanded natural graphite (Timrex *C*-Therm 002 Z11021), consisting of 81 μm particles, IMERYS, were added to the aqueous solution. The slurries were baked for one hour at 80 °C and then heated to 180 °C for one hour to cross-link the binder. Consolidated salt-in-matrix sorbent composites were prepared with 0–15 wt% of graphite flakes or 0–5 wt% of expanded natural graphite as thermally conductive additives. The composition and total mass of the sorbent composites prepared in this study are presented in Table 2. Scanning electron microscope (SEM) images of sorbent composites made with silica gel, $CaCl_2$, PVA and 0, 20 wt.% of graphite flakes or 5 wt.% of expanded natural graphite as conductive additives are shown in Fig. 1(b), Fig. 1(a), and Fig. 1(c), respectively.

2.2. Thermal conductivity and diffusivity measurement

A hot disk transient plane source thermal constant analyzer (TPS 2500S, ThermTest Inc., Fredericton, Canada) capable of precise measurement of thermal conductivity, diffusivity, and specific heat was used for this study. This apparatus uses a transient plane source method following ISO Standard 22,007–2.2 [27]. The testbed measurement setup, including the sample assembly is shown in Fig. 2.

The instrument has different sensor types and software modules to perform bulk material measurements (isotropic and anisotropic), thin films, powders, and liquids. In this study, a bulk sensor (7577) with a 2 mm diameter nickel double spiral insulated in a thin layer of Kapton is used for both transient heating of the sample and temperature measurements. Details of TPS testing can be found elsewhere [8,28]. A humidifier (P-10C-1C-2–0–031,300-v7, Cellkraft AB, Sweden) was connected to the thermal constant analyzer to control the humidity inside the TPS chamber. Also, a heating/cooling circulator was connected to the chamber to maintain a constant controlled temperature.

For bulk material (isotropic) measurements, a sensor was placed on either side of a pair of dried identical samples. After 20 min for temperature and the specified RH humidity equilibration, measurements were performed on each sample three times at different locations, and a standard deviation of 10% was measured.

2.3. Uncertainty analysis

Following the same methodology as [29], the uncertainty of thermal conductivity u_k was calculated as:

$$u_k = \sqrt{u_{k,m}^2 + \sigma_k^2} \tag{1}$$

where, $u_{k,m}$ is the measurement accuracy of the TPS instrument and σ_k is the standard deviation of the measurements. The value of $u_{k,m}$ reported by the manufacturer is 5% of the reading [30].

The uncertainty of diffusivity u_α was calculated identically to conductivity as:

$$u_\alpha = \sqrt{u_{\alpha,m}^2 + \sigma_\alpha^2} \tag{2}$$

where, $u_{\alpha,m}$ is set to be 5% of the reading and σ_α is the standard deviation of the measurements.

2.4. Geometrical parameters of the sorbent composite and additive particles

Geometrical parameters, including the host matrix pore size distribution, and graphite-based additive particle size should be measured to be used as input to the present model. Nitrogen sorption isotherms of the samples were collected with a volumetric physisorption analyzer (Autosorb iQ-MP, Quantachrome Instruments)

Table 2
Composition and total mass of sorbent composite samples.

Name	Silica gel (wt%)	$CaCl_2$ (wt%)	PVA (wt%)	Graphite flake (wt%)	ENG (wt%)	Dry mass (g)
CG0	45	45	10	0	0	7.54
CGF5	42.5	42.5	10	5	0	8.65
CGF10	40	40	10	10	0	8.60
CGF15	35	35	10	15	0	9.00
CENG1	44.5	44.5	10	0	1	10.54
CENG3	43.5	43.5	10	0	3	9.70
CENG5	42.5	42.5	10	0	5	10.80

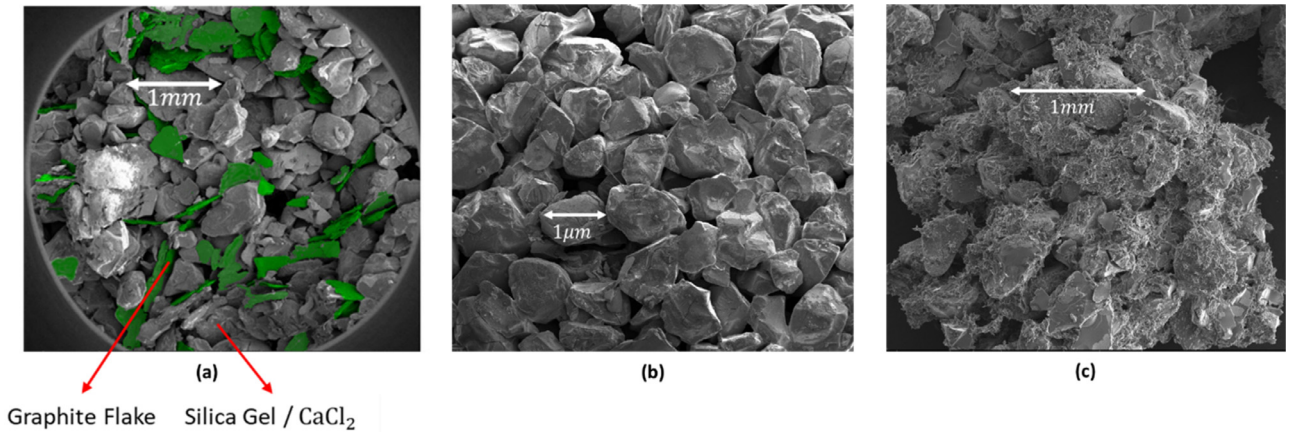

Fig. 1. SEM images of: (a) a sorbent composite made with SG-$CaCl_2$-PVA and 20 wt.% of GF (colored in green) [26]; (b) a sorbent composite made with SG-$CaCl_2$-PVA without conductive additives; and (c) a sorbent composite made with SG-$CaCl_2$-PVA and 5 wt.% of ENG (For interpretation of the references to color in this figure legend, the reader is referred to the web version of this article).

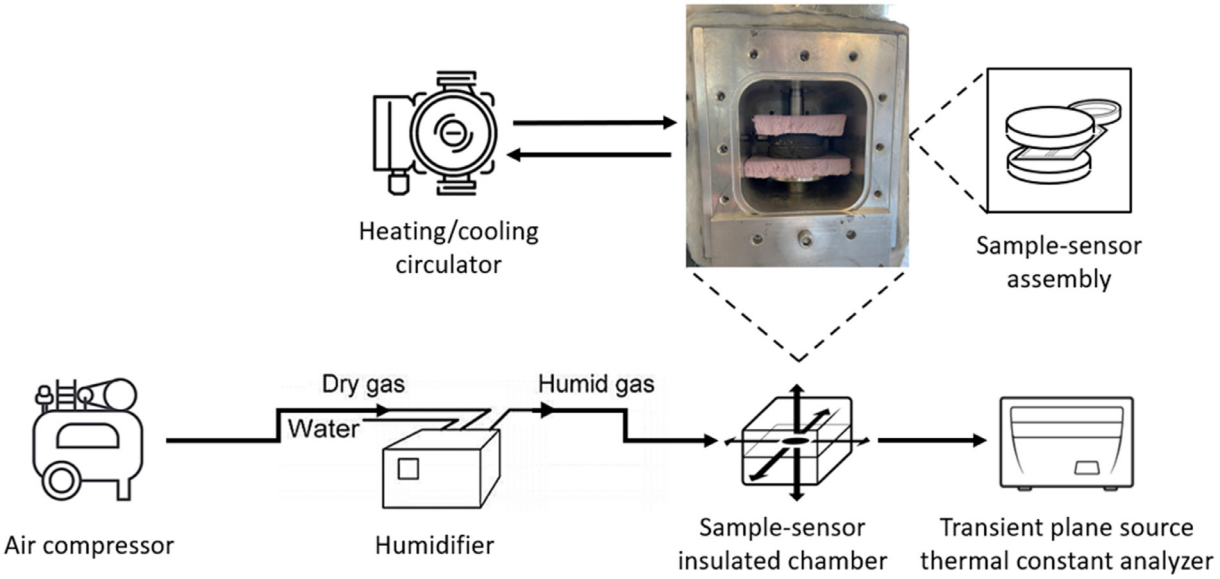

Fig. 2. A schematic of a testbed measurement setup, including an air compressor, humidifier, TPS analyzer instrument, heating/cooling circulators, and a sample-sensor assembly insulated chamber containing RH and temperature sensors.

to determine the average pore diameter (d_p) and pore volume (V). Prior to the testing, the samples were dried under vacuum at 150 °C for 6 h, followed by 2 h at 200 °C.

2.4.1. Pore size distribution

The differential pore volume distribution of the silica and composite samples were obtained through the analysis of the adsorption branch of the N_2 isotherms and shown in Fig. 3. Based on the measured data, the average pore size diameter for silica gel B150 was calculated as $d_p = 16.76$ nm. This average pore size diameter was used as a baseline and was a critical parameter to determine the dimensions of the effective medium unit cell of the present model. It would be also worthwhile to report that the total pore volume, and the surface area per gram were 1.127 cc·g^{-1}, and 268.13 m^2·g^{-1}, respectively.

3. Model development

3.1. Thermal conductivity of the effective medium

In this study, an analytical model for the effective thermal conductivity of the sorbent composite is developed based on a unit cell approach, where the thermal conductivity calculation is made for an elementary cell, shown in Fig. 5(b), as a representative of the entire effective medium. Therefore, the thermal conductivity of the composite is equal to that of the unit cell. It is assumed that the heat conduction in the unit cell is one-dimensional, which leads to the isothermal top and bottom surfaces, while the lateral walls are adiabatic due to symmetry [31]. It is also assumed that the natural convection in the small pores between the sorbents can be neglected [32], and radiation is also negligible at low temperatures (below 600 °C [33]). Therefore, heat transfer occurs via conduction through the solid host matrix and conduction through the interstitial gas.

As shown in the SEM image of Fig. 1(a), and schematically presented in Fig. 4(a), the porous sorbent composite is represented as a periodical structure with a skeleton so that the unit cell with a simple geometry may be segregated. Moreover, due to symmetry, the unit cell here is 1/16 of the periodical cubic structure shown in Fig. 4(b). Following the methodology introduced by Luikov et al. [24] and modified by Bjurstrom et al. [25], some modifications have been made to the unit cell to better represent the morphology of the sorbent composite. Fig. 5(a) shows the unit cell right view, including the main geometrical parameters. The size of the

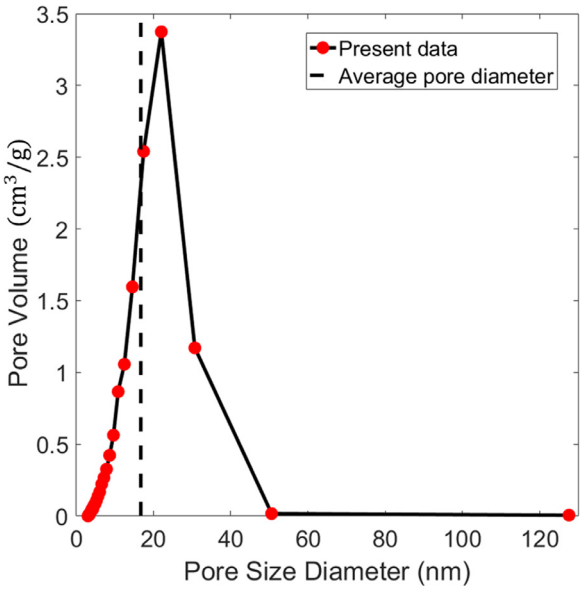

Fig. 3. Pore size distribution for silica gel B150 from N_2 adsorption isotherms collected using a volumetric physisorption analyzer (Autosorb iQ-MP, Quantachrome instruments) in our lab to determine average pore diameter (d_p) and pore volume (V). The dashed line indicates the average pore diameter ($d_p = 16.76$ **nm**).

unit cell depends on the average pore size diameter of the host matrix (d_p).

The model is developed for sorbents consisting of silica gel, salt, binder, and graphite-based additive particles used for both adsorption and absorption. The assumptions used in the development of the present model are:

- Thermodynamic equilibrium of the sorbent composite at each partial pressure. Therefore, the uptake of the sorbent particles corresponds to the equilibrium water uptake at a steady-state temperature and relative humidity (or pressure ratio, P/P_{sat}, for the closed adsorption systems).
- The binder effect is neglected due to its low concentration.
- The contact between graphite additive particles and the sorption material is perfect, i.e., no thermal contact resistance is considered.
- The sorption material and graphite additive particles have constant anisotropic properties, listed in Table 3;.
- Based on a previous study performed in our lab [34], the angle of additive particles (θ) is assumed to be 45 ° This assumption can also be justified by considering the fact that the additive particle distribution in the composite is random (Gaussian distribution), thus the angles could vary from 0 to 90 °.
- Uniform pore size diameter is considered; the average measured pore size is used.
- The absorbed water is considered as a distributed film with a uniform thickness of t_w around the solid skeleton of the host matrix.

Using the above assumptions, a thermal resistance network is developed to represent the heat conduction in the unit cell shown in Fig. 5(c). The first index of the resistances stands for the medium through which heat is flowing, and the second index stands for the length of the path of heat through this medium.

The thermal resistance network consists of: (i) bulk thermal resistance of the solid silica, $R_{S,\frac{l}{2}}$; (ii) resistance of the thermal path consisting of solid silica and absorbed water layers, R_{sw,r_s}, $R_{w,\frac{l_s}{2}}$; (iii) resistance of the thermal path consisting of solid silica, interstitial gas (water vapor), and absorbed water layers, R_{swg,r_w}, $R_{g,\frac{l_w}{2}}$; and (iv) resistance of interstitial gas in the mesopores, and intergranular pores of the sorbent composite, $R_{g,\frac{l}{2}}$.

The thermal resistance for each path is calculated based on the average pore size diameter, measured thermal conductivity, silica gel true density, and water density. The resistance of interstitial gas in the mesopores is calculated using the same method developed by Bahrami et al. [37,38].

Performing an order of magnitude analysis, the thermal resistances in paths (iii) and (iv) are an order of magnitude higher than the first two paths shown in Fig. 5(c). Paths (ii), (iii), and (iv) are 2, 12, and 17 times higher than path (i), respectively. This is due to the considerable difference in the thermal conductivity of water vapor as interstitial gas compared to that of solid silica and liquid water.

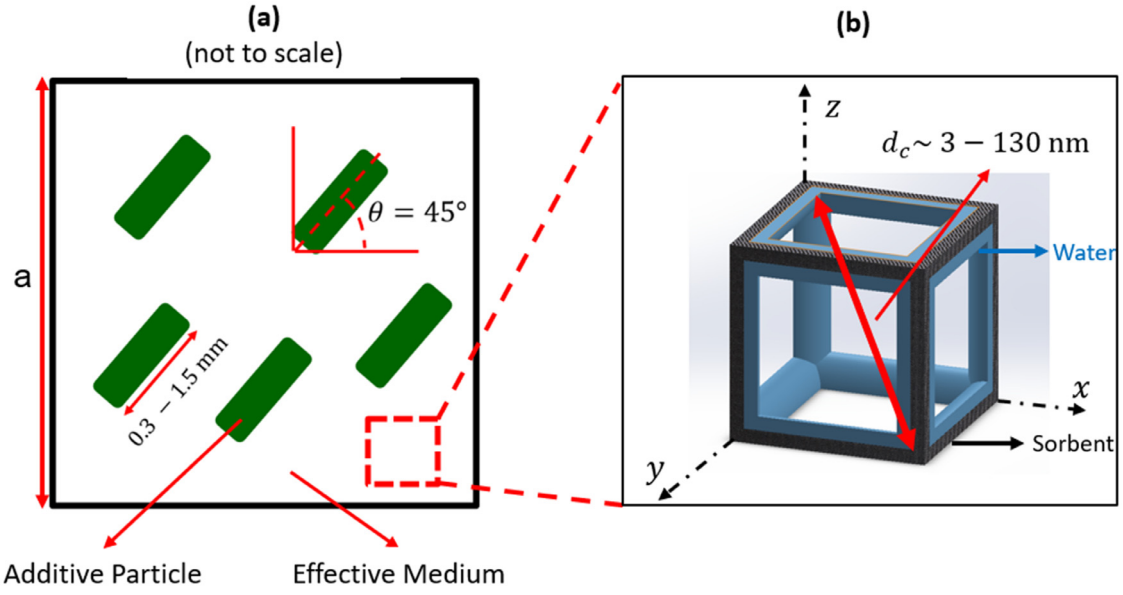

Fig. 4. (a) The effective medium illustration (not-to-scale), thermally conductive particle angle (θ) is assumed to be 45 °, based on [20]; and (b) The silica gel pore unit cell model proposed in this study.

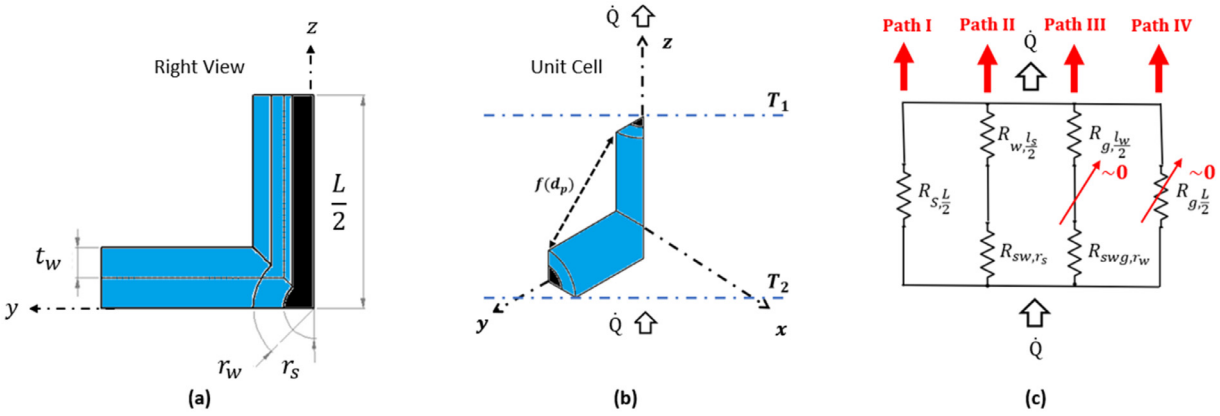

Fig. 5. (a) The right-view schematic of the unit cell, the unit cell here is 1/16 of the periodical cubic structure shown in Fig. 4(b); (b) A schematic illustration of the unit cell; and (c) The thermal resistance network diagram of the unit cell with corresponding thermal paths.

Table 3
Material and geometrical properties of the sorption composites.

Silica gel			Graphite flakes			Expanded Natural graphite		
True density ($g{\cdot}cm^{-3}$) [11]	k_{Silica} ($W{\cdot}m^{-1}{\cdot}K^{-1}$) [11]	Bulk density ($g{\cdot}cm^{-3}$) [34]	$k_{Graphite}$ ($W{\cdot}m^{-1}{\cdot}K^{-1}$) [35]	r_{GF} (μm) [34]	t_{GF} (μm) [34]	Bulk density ($g{\cdot}cm^{-3}$) [36]	r_{ENG} (μm) [36]	t_{ENG} (μm)
2.4	1.35	0.64	8	544	4.3	0.04	40	81

The thermal conductivity and density of the salt solution are calculated based on the mixing rule of effective medium approximation theory using thermal conductivity and density of water, and $CaCl_2$ at 25 °C [39]. However, as the thermal conductivity of water and the saturated salt solution have a slight difference (maximum 8% for the saturated $CaCl_2$ solution), an approximate value of 0.6 $W{\cdot}m^{-1}{\cdot}K^{-1}$ is used in the model.

Though the temperature effect on the thermal conductivity of silica gel and $CaCl_2$ in the studied temperature range (20–120 °C) is negligible, the thermal conductivity of liquid water has a 0.08 $W{\cdot}m^{-1}{\cdot}K^{-1}$ increase (12%) in this temperature range. Further investigation indicates that this difference will result in a 0.7% increase in the thermal conductivity of the effective medium. Therefore, it can also be neglected to simplify the model.

An equivalent cubic diagonal of a spherical shaped object is defined as the diagonal of a cube of equivalent volume. The equivalent cubic diagonal, d_c, for the pore volume is calculated as:

$$d_c = 1.4 \cdot d_p \tag{3}$$

Based on the geometrical assumptions of the unit cell, the solid host matrix radius, r_s, is calculated by solving the following equation using porosity (ε), and the equivalent cubic diagonal (d_c) as follows:

$$\varepsilon = \frac{12\pi\sqrt{3}}{d_c^3} r_s^3 - \frac{9\pi}{d_c^2} r_s^2 + 1 \tag{4}$$

The absorbed water uptake layer thickness, t_w, is also calculated by solving the following equation using the true density (i.e., the quotient of mass over the volume of a sample, without considering pores in the material (true volume).) of solid host matrix and water (ρ_s, ρ_w), water uptake (ω), host matrix radius (r_s), and the equivalent cubic diagonal of the unit cell (d_c) as:

$$\omega = \frac{\rho_w}{\rho_s}\left(\frac{-t_w^3 + \left(\frac{3d_c}{4\sqrt{3}} - 3r_s\right)t_w^2 + \frac{3d_c r_s}{2\sqrt{3}} t_w}{\left(\frac{3d_c}{4\sqrt{3}} - r_s\right)r_s^2}\right) \tag{5}$$

Finally, based on the simplified thermal resistance network of the unit cell, the thermal conductivity of the effective medium of sorbent composite will be estimated by using the calculated equivalent cubic diagonal, host matrix radius and water uptake layer thickness from Eqs. (3)–(5) and the thermal conductivity of the host matrix as below:

$$k_m = \frac{4\sqrt{3}/d_c}{\frac{\frac{d_c}{\sqrt{3}} - 2r_s}{1.2 \times t_w \cdot r_s} - \frac{1.2 \times \left[\arctan\left(\frac{1.2-k_s}{\sqrt{1.2k_s - k_s^2}}\right) - \pi\sqrt{1.2k_s - k_s^2}\right]}{t_w \cdot (k_s - 0.6)\sqrt{1.2k_s - k_s^2}}} \tag{6}$$

For this study, and generally, in the case of using silica gel B150 (B represents the particle size range of 200–500 μm, and 60 represents the average particle size reported by the supplier as 150 Å) as the host matrix, r_s and t_w can be calculated using the following correlations, which are derived for typical porosity range of silica gels (i.e., $0.4 < \varepsilon < 0.8$) and water uptake range of $0.01 < \omega < 0.99$ both fitted with the coefficient of determination of $r^2 = 0.99$.

$$r_s = -6.3\varepsilon + 7.3 \tag{7}$$

$$t_w = 2.4\omega \tag{8}$$

Using Eqs. (7) and (8) in Eq. (6) will further simplify the effective thermal conductivity medium as:

$$k_m = \frac{\omega(16.3 - 14\varepsilon) - 1.4\varepsilon + 2.8}{31.5 - 16\varepsilon} \tag{9}$$

The thermal conductivity of the effective medium is validated with experimental data collected in our lab for sorbent composites made of SG B150, $CaCl_2$, and PVA tested at a RH of 2–70%. As shown in Fig. 6, the model can predict the thermal conductivity of the sorption composite and the increasing trend as a function of water uptake and shows a good agreement with the experimental data with the average and maximum relative differences of 5.72% and 10.66%, respectively.

3.2. Thermal conductivity of the sorbent composite, containing a graphite-based additive particle

Following the methodology introduced by Fayazmanesh et al. [34], the effective thermal conductivity of the sorbent composites

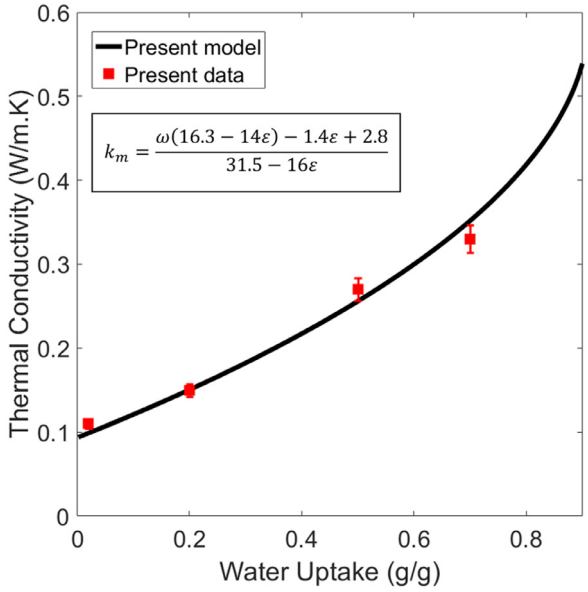

Fig. 6. A comparison between the measured thermal conductivity and analytical model for the sorbent composite CG0, without thermally conductive additives, over a water uptake range of 0.02–0.9 (g·g^{-1}).

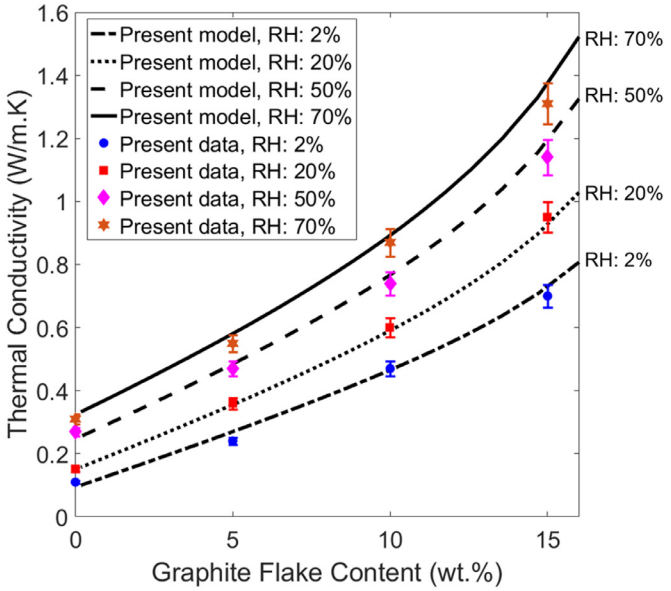

Fig. 7. A comparison between the measured thermal conductivity and analytical model for the consolidated sorbent composites CG0, CGF5, CGF10, CGF15. Samples were measured at 2, 20, 50 and 70% RH.

containing conductive additive particles is calculated assuming that identical disk-shaped additive particles are evenly and randomly dispersed throughout the composite. The host matrix here is the modeled by an effective medium and the host matrix thermal conductivity (k_m), is calculated using the correlations introduced in the previous Section 3.1. In this way, the effect of water uptake, host matrix pore size distribution, sorbent porosity, and the additive particles are taken into account.

In this study graphite flakes and expanded natural graphite are chosen as thermally-conductive additives to the sorbent composite. While thermal conductivity of these additives is similar, worm-like fluffy expanded natural graphite has 16 times smaller bulk density, larger aspect ratio, and smaller particle size and thus is more likely to create enhanced thermal paths to improve the heat transfer in the composite. However, the low density of ENG poses some volumetric challenges like decreasing the specific cooling or heating power per volume and also adversely affects the mechanical strength of sorbent coatings.

The size of the unit cell depends on the volume fraction of additive particles in each sample, and it is calculated using the additive particle dimensions, and the density of particles and effective medium. Therefore, the effective thermal conductivity of the consolidated sorbent composite for additive particle with an angle of $\Theta = 45\ ^\circ$ will be:

$$k_{eff} = \frac{1}{2}\left[\frac{k_m\left[\frac{t_p.k_m}{\phi} + (k_p - k_m)a\right]}{\frac{t_p.k_m}{\phi} + (k_p - k_m)(a - t_p)} + \frac{r_p(2k_pa - \pi r_p(k_p - k_m))}{r_p\left(k_m.\left(a^2 - 2r_pt_p\right)\cdot(2k_pa - \pi r_p(k_p - k_m))\right) + 2t_pa}\right] \quad (10)$$

where, k_p, r_p, t_p are the thermal conductivity, and radius and thickness of the additive particle, respectively, and a is the side length of the cubic unit cell as shown in Fig. 4(a), and calculated as:

$$a = \sqrt[3]{\pi r_p^2 t_p/\phi} \quad (11)$$

4. Results and discussion

The present analytical model for the effective thermal conductivity of consolidated sorbent composites (SG B150, $CaCl_2$, and PVA) containing 0–15 wt.% of graphite flakes or 0–5 wt.% of expanded natural graphite are compared to the measured experimental data of the samples shown in Fig. 7 and Fig. 8, respectively. The analytical model can predict the experimental data rather well with a minimum, maximum and averaged relative difference between the model and data of 0.02%, 7.69%, and 4.15%, respectively.

A parametric study has been carried out to show the variation of the effective thermal conductivity of the sorbent composite with water uptake, sorbent porosity, additive type, and additive content.

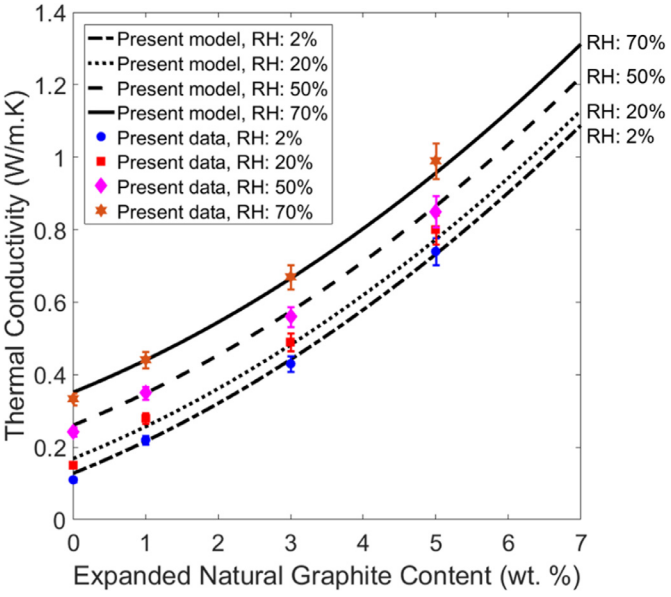

Fig. 8. A comparison between the measured thermal conductivity and analytical model for the consolidated sorbent composites CG0, CENG1, CENG3, CENG5. Samples were measured at 2, 20, 50 and 70% RH.

Table 4
Baseline parameters for the parametric study.

Sorbent composite	RH (%)	ω (g g^{-1})	Sorbent porosity	Additive type	φ (wt.%)
CGF0	2	0.02	0.7	Graphite flakes	0–15

Sorbent material properties and geometrical parameters of the unit cell were considered as a baseline (shown in Table 4) in which each parameter is changed over an arbitrarily chosen range while other parameters were kept constant.

4.1. Impact of additives on the effective thermal conductivity of the sorbent composite

The graphite flakes and expanded natural graphite additives had different distributions in the composite samples, as well as different particle sizes, aspect ratios, and specifically, the order of magnitude difference in their bulk densities. Furthermore, the expanded natural graphite had a significantly more pronounced effect on the effective thermal conductivity of the consolidated sorbent composites. The thermal conductivity of the sorbent composites (CG0, CGF5, CGF10, CGF15) increased from 0.11 to 0.70 $W{\cdot}m^{-1}{\cdot}K^{-1}$ as the graphite flake content was increased from 0 to 15 wt.% when tested with a RH of 2, 536% enhancement, shown in Fig. 7. The addition of 5 wt.% ENG to the sorbent composites (CG0, CENG1, CENG3, CENG5) also increased the thermal conductivity from 0.11 to 0.74 $W{\cdot}m^{-1}{\cdot}K^{-1}$ when tested with a RH of 2%, 572% enhancement, shown in Fig. 8. The reason behind these improvements is that the addition of GF or ENG as thermally-conductive additives lead to forming higher conductivity paths to increase the effective thermal conductivity.

4.2. Water uptake impact on the effective thermal conductivity of sorbent composite

In order to investigate the impact of water uptake on the effective thermal conductivity of the sorbent composite, the effective thermal conductivity of SG, $CaCl_2$, PVA composites made with 0–15 wt.% of graphite flakes has been modeled and shown in Fig. 9. The thermal conductivity of the sorbent composite CG0 increased from 0.11 to 0.46 $W{\cdot}m^{-1}{\cdot}K^{-1}$ as the water uptake was increased from 0.02 to 0.9 ($g{\cdot}g^{-1}$) for the sorbent with 0 wt.% of graphite flakes, 318% enhancement. This increase is due to the relatively higher thermal conductivity of water in comparison to the host matrix and water vapor which eventually form thermal paths with less thermal resistance. The result shows a good agreement with the experimental data with the average and maximum relative differences of 5.72% and 10.66%, respectively.

4.3. Impact of water uptake and additives on the thermal diffusivity of the sorbent composite

To investigate the effects of water uptake and additive on the thermal diffusivity (α) of the sorbent composites, the thermal diffusivity of SG, $CaCl_2$, PVA composites were made with 0–15 wt.% of graphite flakes has been modeled using the following equation and compared with the sample's measurements in Fig. 10. The result shows a good agreement with the experimental data with the average and maximum relative differences of 2.49% and 7.96%, respectively.

$$\alpha = \frac{k}{\rho \cdot c_p} \tag{12}$$

where, ρ is sorbent composite bulk density, and c_p is the specific heat capacity.

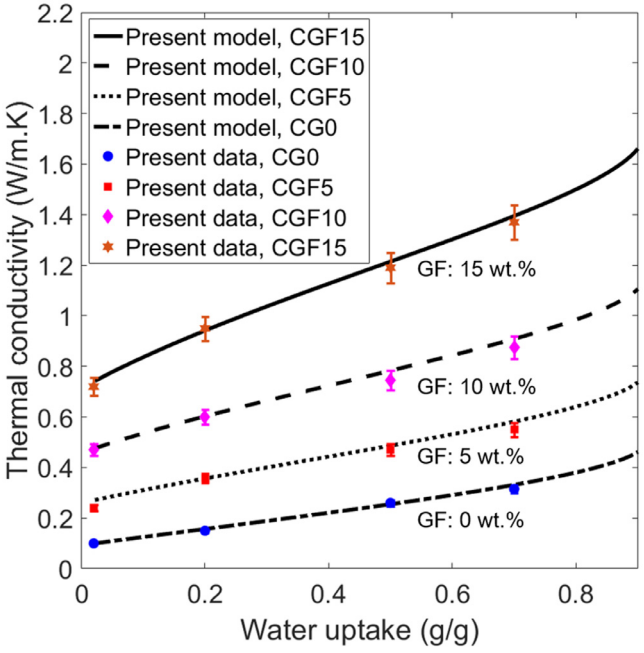

Fig. 9. The water uptake variation impact on the effective thermal conductivity of consolidated sorbents CG0, CGF5, CGF10, and CGF15.

The thermal diffusivity of the sorbent composites (namely, CG0, CGF5, CGF10, and CGF15) increased from 0.12 to 0.90 $mm^2{\cdot}s^{-1}$ as the graphite flake content was increased from 0 to 15 wt.% when tested with a RH of 2%, an 650% enhancement. This significant increase occurs because adding additive content not only increases the effective thermal conductivity of the consolidated composite, but also decreases the bulk density and specific heat capacity of the composite.

On the other hand, though increasing water uptake raises the effective thermal conductivity of the sorbent composite, it also increases the bulk density and specific heat capacity of the composite which eventually leads to a less significant increase in the thermal diffusivity. Therefore, as the water uptake was increased from 0.02 to 0.9 ($g{\cdot}g^{-1}$) for the sorbent composite CGF15 with a 15 wt.% of graphite flakes, the thermal diffusivity of the sorbent composites increased from 0.90 to 1.20 $mm^2{\cdot}s^{-1}$, 33% enhancement.

4.4. Impact of porosity on the effective thermal conductivity of sorbent composite

After the model is validated with several data sets, we can use the present model with a degree of confidence to predict the impact of other key parameters, such as silica gel porosity on the effective thermal conductivity of the sorbent composite, the effective thermal conductivity of SG, $CaCl_2$, PVA composites made with 0–15 wt.% of graphite flakes has been modeled and shown in Fig. 11. The result shows a good agreement with the experimental data with the average and maximum relative differences of 9.22% and 12.7%, respectively.

The thermal conductivity of the sorbent composite CG0 increased from 0.03 to 0.41 $W{\cdot}m^{-1}{\cdot}K^{-1}$ as the porosity was de-

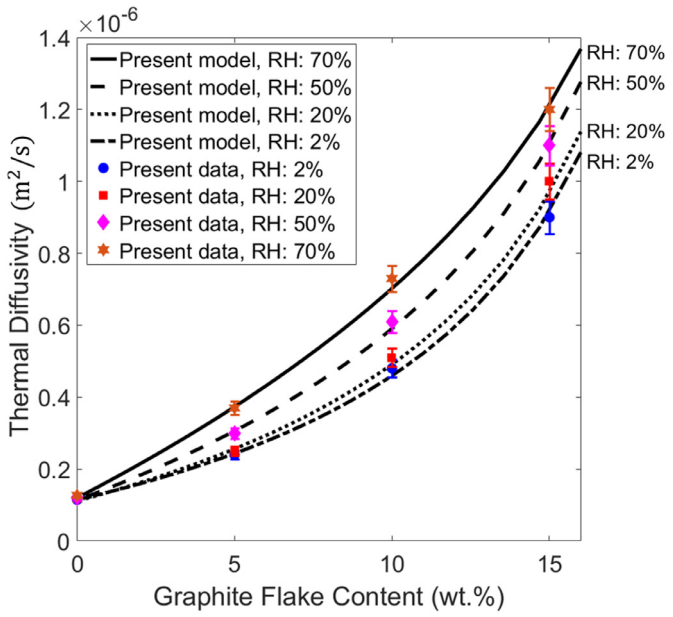

Fig. 10. A comparison between the measured thermal diffusivity and analytical model for consolidated sorbent composites CG0, CGF5, CGF10, CGF15. Samples were measured at 2, 20, 50, and 70% RH.

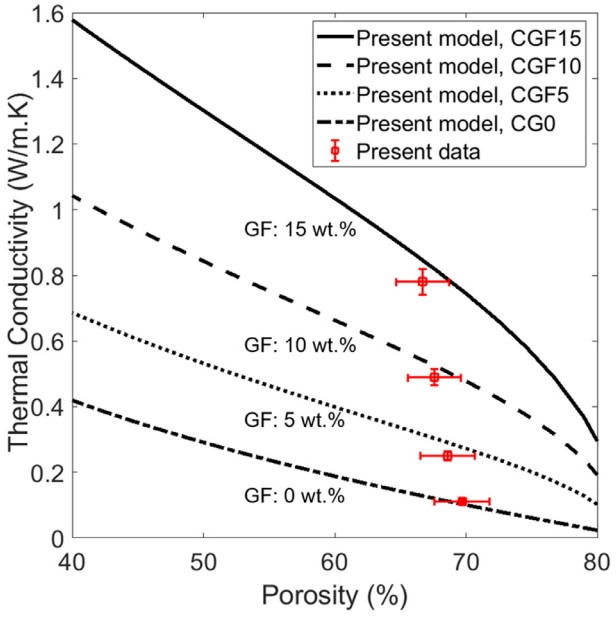

Fig. 11. The porosity variation impact on the effective thermal conductivity of consolidated sorbents CG0, CGF5, CGF10, CGF15, when tested with 2% RH.

creased from 80 to 40% for the sorbent with 0 wt.% of graphite flakes at 2% RH, 1200% enhancement. Nevertheless, it is important to note that decreasing porosity, depending on the case, can reduce the water uptake capacity, which adversely impacts the sorption kinetics. Therefore, performing optimization is necessary to choose the porosity of silica gel.

The porosity of the sorbent composites CG0, CGF5, CGF10, and CGF15 are calculated based on their measured bulk densities, weight percentage and true density of silica, $CaCl_2$, PVA, and graphite flakes in each composite. The uncertainty of porosity calculations measured to be 6%.

5. Conclusion

A new analytical quasi-steady-state model to estimate the effective thermal conductivity and thermal diffusivity of wetted sorbent composites containing thermally-conductive additives has been developed that considers all salient morphological parameters, material properties, and operating conditions. This included thermal conductivity, specific heat capacity, and density of the sorbent and additive materials, host matrix pore size distribution, porosity, thermally conductive additive type and content, water uptake, and temperature to predict the effective thermal conductivity and thermal diffusivity of the consolidated sorbent composite under the normal operating condition of an adsorption or absorption system. This model was developed for silica gel-based composites, however; the proposed methodology can be extended and applied to other sorts of sorption composites made with meso–porous host matrix with constant anisotropic thermophysical properties over the typical operating condition of sorption systems as well.

Several consolidated salt-in-matrix sorbents were fabricated with silica gel, $CaCl_2$, PVA binder, and 0–15 wt.% of graphite flakes and with 0–5 wt.% of expanded natural graphite as thermally conductive additives. The model has been successfully validated with the measured thermal conductivity of our sorbent samples collected at 25 °C with 2, 20, 50, and 70% RH.

The results showed that the addition of 15 wt.% of graphite flakes or 5 wt.% of expanded natural graphite into consolidated sorbents lead to a 536% (from 0.11 to 0.70 $W{\cdot}m^{-1}{\cdot}K^{-1}$), and 572% (from 0.11 to 0.74 $W{\cdot}m^{-1}{\cdot}K^{-1}$) increase in thermal conductivity, respectively, when tested at 2% RH and 25 °C. It was also shown that the thermal conductivity of the sorbent composite CG0 increased from 0.11 to 0.46 $W{\cdot}m^{-1}{\cdot}K^{-1}$ ($a \sim 318\%$ enhancement), as the water uptake was increased from 0.02 to 0.9 ($g{\cdot}g^{-1}$).

Furthermore, a comprehensive parametric study was performed investigating the impact of water uptake, porosity, pore size, thermally conductive additive type, and additive content on the effective thermal conductivity and thermal diffusivity of the consolidated sorbent composite. This study showed that the thermal diffusivity of the sorbent composites (CG0, CGF5, CGF10, CGF15) increased from 0.12 to 0.90 $mm^2{\cdot}s^{-1}$ as the graphite flake content was increased from 0 to 15 wt.% when tested with a RH of 2%, i.e., an 650% improvement.

The present analytical model provides a reliable and easy-to-use compact relationship that can be utilized as a useful tool to enhance the heat transfer and overall performance of sorption systems.

Declaration of Competing Interest

The authors declare that they have no known competing financial interests or personal relationships that could have appeared to influence the work reported in this paper.

CRediT authorship contribution statement

A. Shafiepour: Conceptualization, Methodology, Validation, Investigation, Writing – original draft, Visualization. **C. McCague:** Resources, Writing – review & editing. **M. Bahrami:** Conceptualization, Supervision, Funding acquisition, Writing – review & editing.

Acknowledgments

The authors gratefully acknowledge the financial support of the Innovate BC, and the Natural Sciences and Engineering Research Council of Canada (NSERC) through the Collaborative Research and Development Grant (CRDPJ 488777–15). The SEM studies were conducted at Simon Fraser University's 4D LABS facility

with the assistance of their technical staff. The 4D LABS shared facilities are supported by Canada Foundation for Innovation (CFI), British Columbia Knowledge Development Fund (BCKDF), Western Economic Diversification Canada (WD), and Simon Fraser University (SFU).

Appendix. Detailed calculations of thermal resistance model development

The thermal resistance for each path is calculated based on the average pore size diameter, measured thermal conductivity, silica gel true density (i.e., the quotient of mass over the volume of a sample, without considering pores in the material (true volume)), and water density. The resistance of interstitial gas in the mesopores is calculated using the same method developed by Bahrami et al. [37,38].

The first index of the resistances stands for the medium through which heat is flowing, and the second index stands for the length of the path of heat through this medium.

To calculate the thermal resistances, First, three additional parameters defined as:

$$l_s = L - 2r_s \tag{13}$$

$$l_w = L - 2r_w \tag{14}$$

$$r_w = r_s + t_w \tag{15}$$

In thermal path (i), for conduction through the solid silica, $R_{S,\frac{L}{2}}$ defined as:

$$R_{s,\frac{L}{2}} = \frac{L/2}{k_s.\left(\frac{\pi r_s^2}{8}\right)} \tag{16}$$

Next, in path (iv), for the conduction through the water vapor gas phase in pores, $R_{g,\frac{L}{2}}$ defined as:

$$R_{g,\frac{L}{2}} = \frac{L/2}{k_g.l_w^2/8} \tag{17}$$

Path (ii) consists of two series of thermal resistances. The first one, R_{sw,r_s}, represents the combined solid/liquid water phase, which is indicated with two parallel resistances labeled; R_s, and R_w, respectively. The corresponding thermal resistance diagram and schematic of path (ii) is shown in Fig. A.2. Defining the horizontal element dy, we have:

$$y = rcos\theta_s \tag{18}$$

$$dy = -rsin\theta_s d\theta_s \tag{19}$$

$$R_s = \int_y^0 \frac{dy}{k_s.(rsin\theta_s).\frac{l}{2}} \tag{20}$$

$$R_w = \int_y^0 \frac{dy}{k_w.(r - rsin\theta_s).\frac{l}{2}} \tag{21}$$

therefore, R_{sw,r_s} is calculated using the following:

$$\frac{1}{R_{sg,r}} = \frac{1}{R_s} + \frac{1}{R_g} \tag{22}$$

by integrating the dy element for $(0, y)$, R_{sw,r_s} is calculated as:

$$R_{sw,r_s} = \frac{1}{t_w}\int_0^{\frac{\pi}{2}} \frac{sin\theta_s d\theta_s}{(k_s \cdot sin\theta_s + k_w \cdot (1 - sin\theta_s))} \tag{23}$$

The second thermal resistance in this path, which represents the thermal resistance to conduction through the above liquid water phase, $R_{w,\frac{l_s}{2}}$, is written as:

$$R_{w,\frac{l_s}{2}} = \frac{l_s/2}{k_w.\frac{\pi}{8}.\left(r_w^2 - r_s^2\right)} \tag{24}$$

Thermal path (iii) is quite similar to path (ii) except that it consists of three solid, liquid, and gas phases each representing with a parallel resistance naming; $R_{s'}$, $R_{w'}$, and $R_{g'}$, respectively. The corresponding thermal resistance diagram and side-view schematic for this path is shown in Fig. A.3. Following the same methodology used in path (ii), the horizontal element dy' is defined:

$$y' = r_s \cos(\theta_s) = r_w \cos(\theta_w) \tag{25}$$

$$dy' = -r_s sin\theta_s d\theta_s \tag{26}$$

The thermal resistances for each layer are written as:

$$R_{s'} = \int_y^0 \frac{dy'}{k_s.(rsin\theta).\frac{l_w}{2}} = \int_0^{\frac{\pi}{2}} \frac{r_s Sin\theta_s d\theta}{k_s r_s Sin\theta_s.\frac{l_w}{2}} = \frac{\pi}{k_s l_w} \tag{27}$$

$$R_{w'} = \int_y^0 \frac{dy'}{k_w r_w Sin\theta_w.\frac{l_w}{2}} \tag{28}$$

$$R_{g'} = \int_y^0 \frac{dy'}{k_g.(r_w - r_w sin\theta_w).\frac{l_w}{2}} \tag{29}$$

consequently, for conduction through the combined solid/liquid/gas, R_{swg,r_w} is calculated as:

$$R_{swg,r_w} = \left(\frac{1}{R_s} + \frac{1}{R_w} + \frac{1}{R_g}\right)^{-1} \tag{30}$$

integrating the dy' element for $(0, y')$ results in:

$$R_{swg,r_w} = \frac{k_s l_w}{\pi} + \left(\frac{2}{l_w}\int_0^{\frac{\pi}{2}} \frac{sin\theta_w d\theta_w}{(k_w.sin\theta_w + k_g.(1 - sin\theta_w))}\right)^{-1} \tag{31}$$

The other thermal resistance in path (iii), which represents the resistance to conduction through the pore area above the uptake layer, $R_{g,l_w/2}$, is calculated as:

$$R_{g,l_w/2} = \frac{l_w/2}{kg.\frac{l_w}{2}.r_w} = \frac{4}{k_g.r_w} \tag{32}$$

Performing an order of magnitude analysis shown in Fig. A.4, the thermal resistances in paths (iii) and (iv) are an order of magnitude higher than the first two paths shown in Fig. A.1(b). This is due to the considerable difference in the thermal conductivity of water vapor as interstitial gas compared to that of solid silica and liquid water. Therefore, the simplified thermal resistance network shown in Fig. A.5 will include thermal paths (i) and (ii) only.

The thermal conductivity and density of the salt solution are calculated based on the mixing rule of effective medium approximation theory using thermal conductivity and density of water, and $CaCl_2$ at 25 °C [39]. However, as the thermal conductivity of water and the saturated salt solution have a slight difference (maximum 8% for the saturated $CaCl_2$ solution), an approximate value of 0.6 $W{\cdot}m^{-1}{\cdot}K^{-1}$ is used in the model.

Though the temperature effect on the thermal conductivity of silica gel and $CaCl_2$ in the studied temperature range (20–120 °C) is negligible, the thermal conductivity of liquid water has a 0.08 $W{\cdot}m^{-1}{\cdot}K^{-1}$ increase (12%) in this temperature range. Further investigation indicates that this difference will result in a 0.7% increase in the thermal conductivity of the effective medium. Therefore, it can also be neglected to simplify the model.

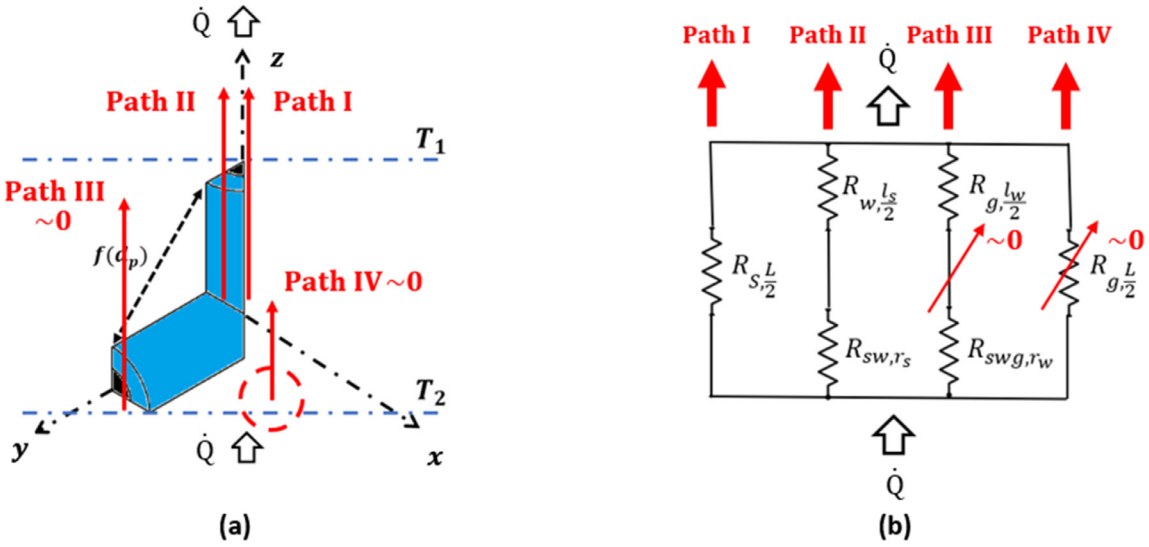

Fig. A.1. (a) An illustation of thermal paths in the unit cell; and (b) The thermal resistance network diagram of the unit cell with corresponding thermal paths.

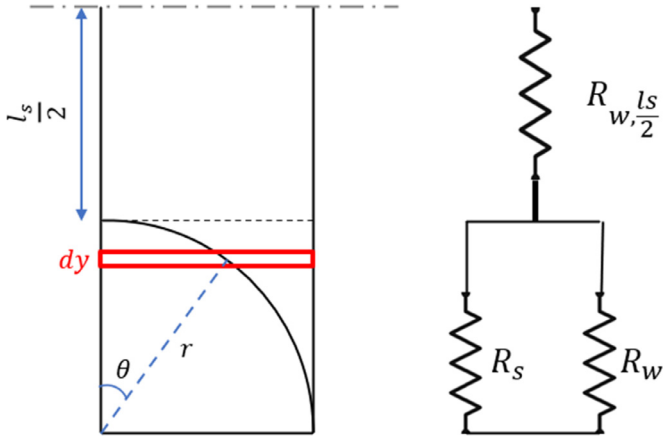

Fig. A.2. The side-view illustration and thermal resistance diagram of the combined solid/liquid phase in thermal path (ii) of Fig. A.1.

As shown in Fig. A.6, an equivalent cubic diagonal of a spherical-shaped object is defined as the diagonal of a cube of equivalent volume. The equivalent cubic diagonal, d_{eq}, for the pore volume is calculated as:

$$d_c = 1.396 \cdot d_p \tag{33}$$

Based on the geometrical assumptions of the unit cell, the solid host matrix radius, r_s, is calculated by solving the following equation using porosity (ε), and d_c as follows:

$$\varepsilon = \frac{12\pi\sqrt{3}}{d_c^3} r_s^3 - \frac{9\pi}{d_c^2} r_s^2 + 1 \tag{34}$$

The absorbed water uptake layer thickness, t_w, is also calculated by solving the following equation using the true density of solid host matrix and water (ρ_s, ρ_w), ω, r_s, d_c as:

$$\omega = \frac{\rho_w}{\rho_s}\left(\frac{-t_w^3 + \left(\frac{3d_c}{4\sqrt{3}} - 3r_s\right)t_w^2 + \frac{3d_c r_s}{2\sqrt{3}} t_w}{\left(\frac{3d_c}{4\sqrt{3}} - r_s\right)r_s^2}\right) \tag{35}$$

Finally, based on the simplified thermal resistance network of the unit cell, the thermal conductivity of the effective medium of sorbent composite is calculated and simplified using MAPLE soft-

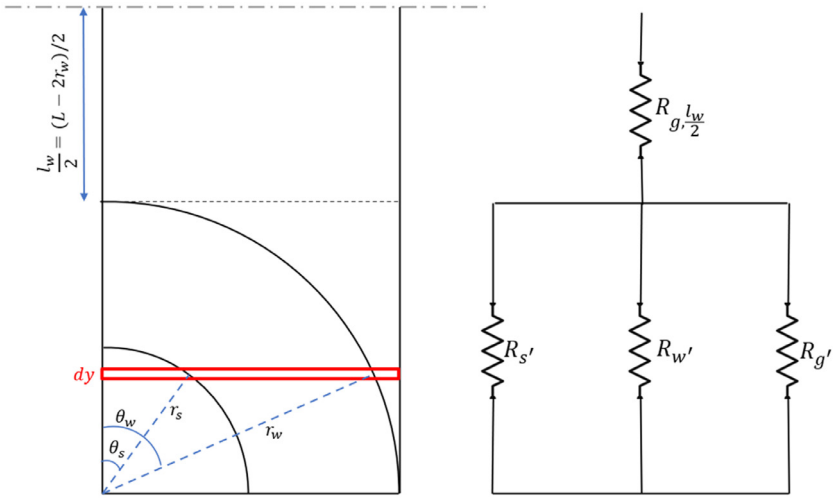

Fig. A.3. The side-view illustration and thermal resistance diagram of the combined solid/liquid/gas phase in thermal path (iii) of Fig. A.1.

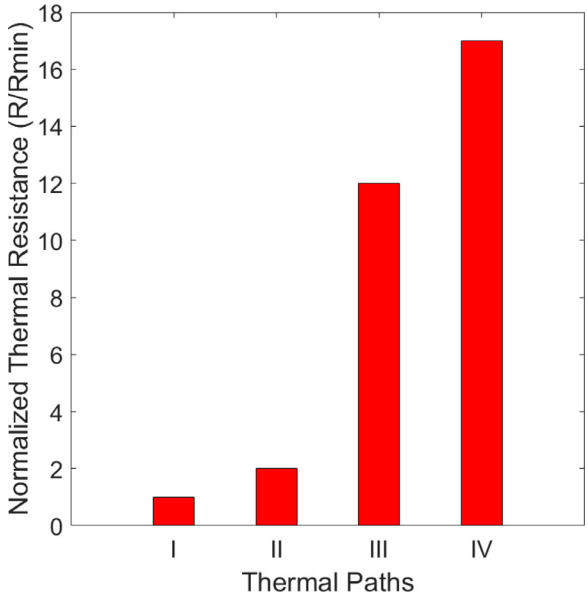

Fig. A.4. An order of magnitude analysis of thermal resistances in the thermal resistance network of the unit cell.

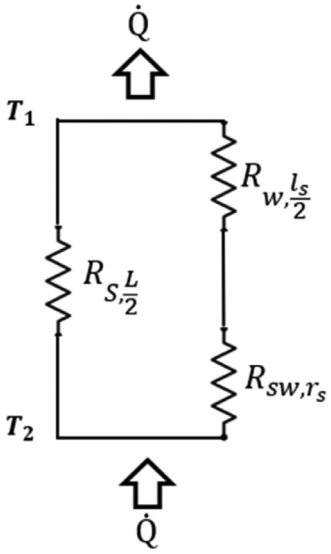

Fig. A.5. A simplified thermal resistance network diagram of the unit cell.

ware as:

$$k_m = \frac{4\sqrt{3}/d_c}{\frac{\frac{d_c}{\sqrt{3}}-2r_s}{1.2\times t_w\cdot r_s} - \frac{1.2\times\left[\arctan\left(\frac{1.2-k_s}{\sqrt{1.2k_s-k_s^2}}\right)-\pi\sqrt{1.2k_s-k_s^2}\right]}{t_w\cdot(k_s-0.6)\sqrt{1.2k_s-k_s^2}}} \tag{36}$$

For this study, and generally, in the case of using silica gel B150 (B represents the particle size range of 200–500 μm, and 60 represents the average particle size reported by the supplier as 150 Å) as the host matrix, r_s and t_w can be calculated using the following correlations, which are derived for typical porosity range of silica gels (i.e., $0.4 < \varepsilon < 0.8$) and water uptake range of $0.01 < \omega < 0.99$ both fitted with the coefficient of determination of $r^2 = 0.99$.

$$r_s = -6.3\varepsilon + 7.3 \tag{37}$$

$$t_w = 2.4\omega \tag{38}$$

Using Eqs. (25) and (26) in Eq. (24) will further simplify the effective thermal conductivity medium as:

$$k_m = \frac{\omega(16.3-14\varepsilon)-1.4\varepsilon+2.8}{31.5-16\varepsilon} \tag{39}$$

To summarize the model development for the effective thermal conductivity of consolidated sorbent composites with conductive additive particles, an algorithm flowchart is designed and presented in Fig. A.7.

Thermal conductivity of the sorbent composite, including a conductive additive particle

Following the methodology introduced by Fayazmanesh et al. [34], the effective thermal conductivity of the sorbent composites containing conductive additive particles is calculated assuming that identical disk-shaped additive particles are evenly and randomly dispersed throughout the composite. The host matrix here is the modeled by an effective medium and the effective medium thermal conductivity (k_m), is calculated using the correlations introduced in the previous Section. In this way, the effect of water uptake, host matrix pore size distribution, porosity, and the additive particles are taken into account.

The size of the unit cell depends on the volume fraction of additive particles in each sample, and it is calculated using the additive particle dimensions, and the density of particles and effective medium. Therefore, the effective thermal conductivity of the consolidated sorbent composite for an additive particle with an angle of $\Theta = 45$ °will be:

$$k_{eff} = \frac{1}{2}\left[\frac{k_m\left[\frac{t_p.k_m}{\varphi}+(k_p-k_m)a\right]}{\frac{t_p.k_m}{\varphi}+(k_p-k_m)(a-t_p)} + \frac{r_p(2k_pa-\pi r_p(k_p-k_m))}{r_p\left(k_m.\left(a^2-2r_pt_p\right)\cdot(2k_pa-\pi r_p(k_p-k_m))\right)+2t_pa}\right] \tag{40}$$

where, k_p, r_p, t_p are the thermal conductivity, and radius and thickness of the additive particle, respectively, and a is the side length of the cubic unit cell as shown in Fig. A.8. A schematic illustration

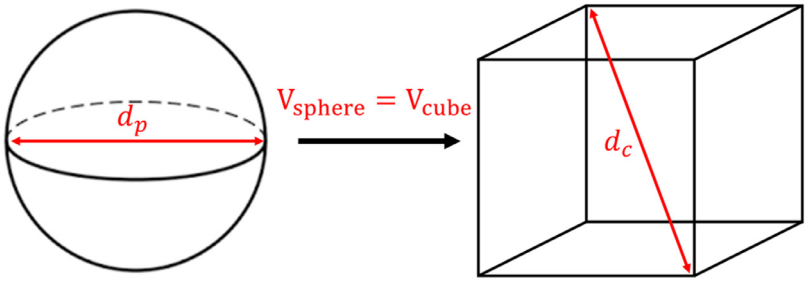

Fig. A6. Schematic illustration of an equivalent cubic diagonal of a spherical-shaped object.

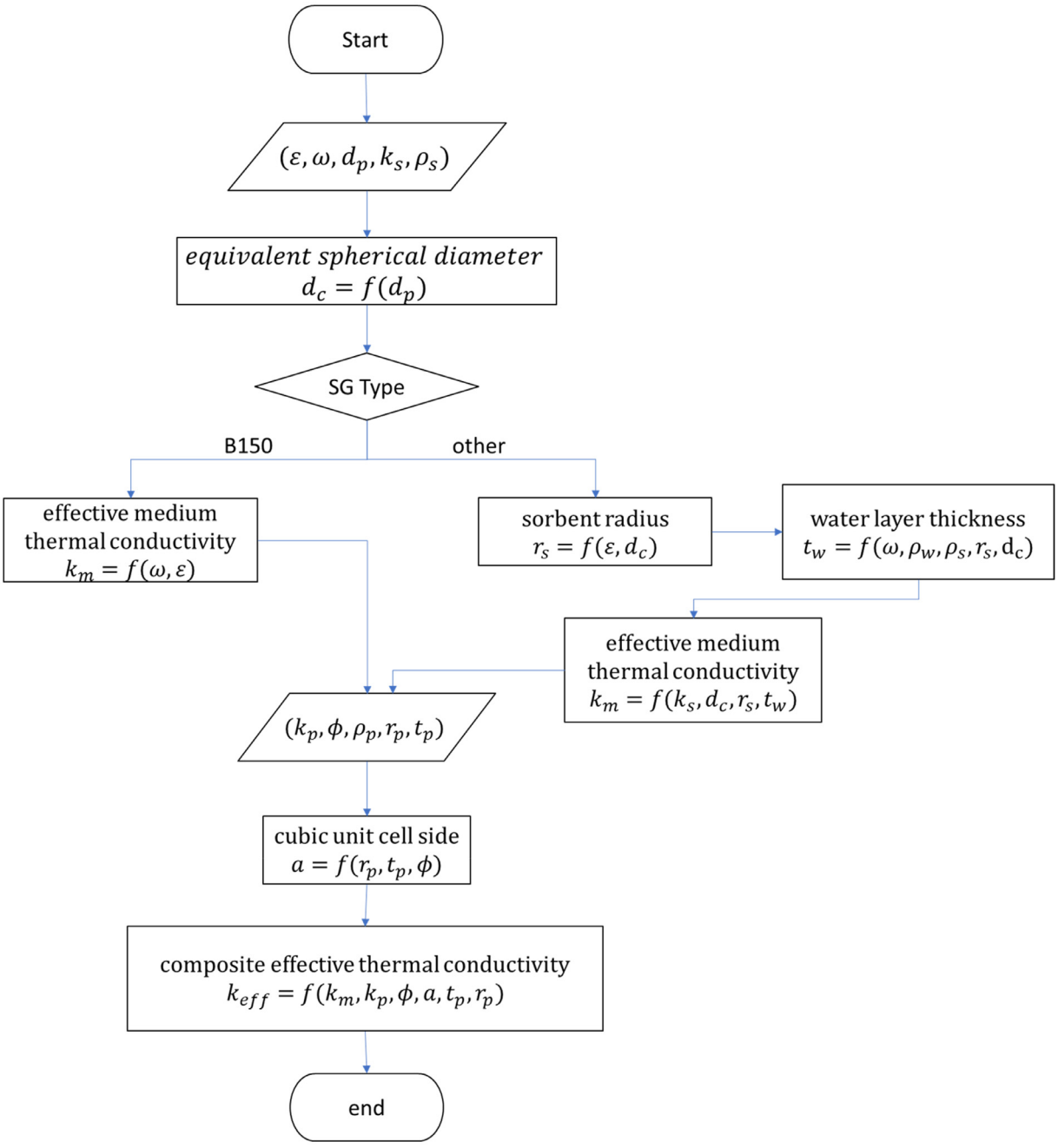

Fig. A.7. An algorithm flowchart for the present analytical model.

of an effective medium composite with conductive additive particle cubic unit cell, and calculated as:

$$a = \sqrt[3]{\pi r_p^2 t_p / \varphi} \tag{41}$$

A MATLAB code is developed to calculate the thermal resistances, solve the equations, and estimate the effective thermal conductivity and thermal diffusivity of consolidated sorbent composites based on the algorithm shown in Fig. A.7 as a function of the measured input parameters.

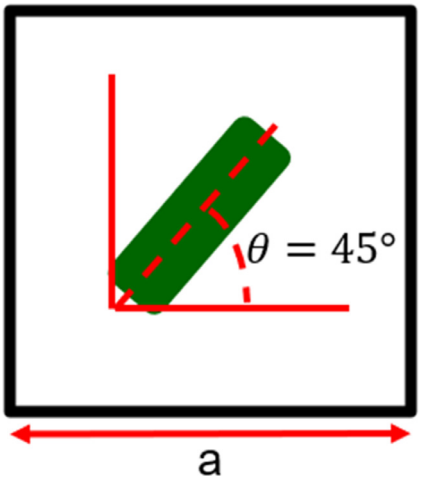

Fig. A.8. A schematic illustration of an effective medium composite with conductive additive particle cubic unit cell.

References

[1] "IEA (2018), The future of cooling, IEA, international energy agency, 2018. [Online]. Available: https://www.iea.org/reports/the-future-of-cooling. [Accessed: 19-Apr-2021].

[2] "Net zero by 2050 plan for energy sector is coming-analysis-IEA." [Online]. Available: https://www.iea.org/commentaries/net-zero-by-2050-plan-for-energy-sector-is-coming. [Accessed: 27-Apr- 2021].

[3] J.M. Pinheiro, S. Salústio, J. Rocha, A.A. Valente, C.M. Silva, Adsorption heat pumps for heating applications, Renew. Sustain. Energy Rev. 119 (2020) 109528 Elsevier Ltd01-Mar-.

[4] F. Meunier, Adsorptive cooling: a clean technology, Clean Prod. Process. 3 (1) (2001) 0008–0020 Jun.

[5] L.F. Cabeza, A. Solé, C. Barreneche, Review on sorption materials and technologies for heat pumps and thermal energy storage, Renew. Energy 110 (2017) 3–39 Sep.

[6] S. Mauran, P. Prades, F. L'Haridon, Heat and mass transfer in consolidated reacting beds for thermochemical systems, Heat Recover. Syst. CHP 13 (4) (1993) 315–319 Jul.

[7] K. Wang, J.Y. Wu, R.Z. Wang, L.W. Wang, Effective thermal conductivity of expanded graphite-$CaCl_2$ composite adsorbent for chemical adsorption chillers, Energy Convers. Manag. 47 (13–14) (2006) 1902–1912 Aug.

[8] K. Fayazmanesh, C. McCague, M. Bahrami, Consolidated adsorbent containing graphite flakes for heat-driven water sorption cooling systems, Appl. Therm. Eng. 123 (2017) 753–760.

[9] T.H. Eun, H.K. Song, J. Hun Han, K.H. Lee, J.N. Kim, Enhancement of heat and mass transfer in silica-expanded graphite composite blocks for adsorption heat pumps: part I. Characterization of the composite blocks, Int. J. Refrig. 23 (1) (2000) 64–73 Jan.

[10] X. Zheng, L.W. Wang, R.Z. Wang, T.S. Ge, T.F. Ishugah, Thermal conductivity, pore structure and adsorption performance of compact composite silica gel, Int. J. Heat Mass Transf. 68 (2014) 435–443 Jan.

[11] Y.Y. Tanashev, A.V. Krainov, Y.I. Aristov, Thermal conductivity of composite sorbents 'salt in porous matrix' for heat storage and transformation, Appl. Therm. Eng. 61 (2) (2013) 401–407.

[12] M. Tatlier, B. Tantekin-Ersolmaz, A. Erdem-Şenatalar, A novel approach to enhance heat and mass transfer in adsorption heat pumps using the zeolite-water pair, Microporous Mesoporous Mater. 27 (1) (1999) 1–10 Jan.

[13] M. Pons, Y. Feng, Characteristic parameters of adsorptive refrigeration cycles with thermal regeneration, Appl. Therm. Eng. 17 (3) (1997) 289–298 Mar.

[14] H.T. Chua, K.C. Ng, A. Malek, T. Kashiwagi, A. Akisawa, B.B. Saha, Modeling the performance of two-bed, silica gel-water adsorption chillers, Int. J. Refrig. 22 (3) (1999) 194–204 May.

[15] L. Marletta, G. Maggio, A. Freni, M. Ingrasciotta, G. Restuccia, A non-uniform temperature non-uniform pressure dynamic model of heat and mass transfer in compact adsorbent beds, Int. J. Heat Mass Transf. 45 (16) (2002) 3321–3330 May.

[16] Y.I. Aristov, G. Restuccia, G. Cacciola, M.M. Tokarev, Selective water sorbents for multiple applications, 7. Heat conductivity of $CaCl_2$-SiO_2 composites, React. Kinet. Catal. Lett. 65 (2) (1998) 277–284.

[17] J.J. Healy, J.J. de Groot, J. Kestin, The theory of the transient hot-wire method for measuring thermal conductivity, Phys. B+C 82 (2) (1976) 392–408 Apr.

[18] A. Freni, M.M. Tokarev, G. Restuccia, A.G. Okunev, Y.I. Aristov, Thermal conductivity of selective water sorbents under the working conditions of a sorption chiller, Appl. Therm. Eng. 22 (14) (2002) 1631–1642 Oct.

[19] G. Buonanno, A. Carotenuto, The effective thermal conductivity of a porous medium with interconnected particles, Int. J. Heat Mass Transf. 40 (2) (1997) 393–405 Jan.

[20] A.J.H. McGaughey, M. Kaviany, Thermal conductivity decomposition and analysis using molecular dynamics simulations part II. Complex silica structures, Int. J. Heat Mass Transf. 47 (8–9) (2004) 1799–1816 Apr.

[21] X. Lu, Y. Zhao, G. Wang, X. Zhu, Effects of structure characteristics and fluid on the effective thermal conductivity of sintered copper foam, Results Phys 19 (2020) 103655 Dec.

[22] B. Dawoud, M.I. Sohel, A. Freni, S. Vasta, G. Restuccia, On the effective thermal conductivity of wetted zeolite under the working conditions of an adsorption chiller, Appl. Therm. Eng. 31 (14–15) (2011) 2241–2246.

[23] Y.Y. Tanashev, Y.I. Aristov, Thermal conductivity of a silica gel + calcium chloride system: the effect of adsorbed water, J. Eng. Phys. Thermophys. 73 (5) (2000) 893–901.

[24] A.V. Luikov, A.G. Shashkov, L.L. Vasiliev, Y.E. Fraiman, Thermal conductivity of porous systems, Int. J. Heat Mass Transf. 11 (2) (1968) 117–140 Feb.

[25] H. Bjurström, E. Karawacki, B. Carlsson, Thermal conductivity of a microporous particulate medium: moist silica gel, Int. J. Heat Mass Transf. 27 (11) (1984) 2025–2036.

[26] H. Bahrehmand, M. Khajehpour, M. Bahrami, Finding optimal conductive additive content to enhance the performance of coated sorption beds: an experimental study, Appl. Therm. Eng. 143 (2018) 308–315 July.

[27] ISO 22007, "International standard conductivity and thermal diffusivity," Int. Stand. ISO 22007-12017(E), vol. 2017, 2017.

[28] S.E. Gustafsson, Transient plane source techniques for thermal conductivity and thermal diffusivity measurements of solid materials, Rev. Sci. Instrum. 62 (3) (1991) 797–804 Mar..

[29] M. Cermak, Natural Graphite Sheet Heat Sinks for Power Electronics, Simon Fraser University, 2020.

[30] H.D. Ab, "Hot disk thermal constants analyzer instruction manual," 2013.

[31] M. Bahrami, M.M. Yovanovich, J.R. Culham, Effective thermal conductivity of rough spherical packed beds, Int. J. Heat Mass Transf. 49 (19–20) (2006) 3691–3701 Sep..

[32] E. Tsotsas, H. Martin, Thermal conductivity of packed beds: a review, Chem. Eng. Process. 22 (1) (1987) 19–37 Jul..

[33] M.M. Yovanovich, E.E. Marotta, Thermal Spreading and Contact Resistances, in: A. Bejan, A.D. Kraus (Eds.), Heat Transfer Handbook, John Wiley & Sons, Inc., Hoboken, 2003, pp. 261–393.

[34] K. Fayazmanesh, S. Salari, M. Bahrami, Effective thermal conductivity modeling of consolidated sorption composites containing graphite flakes, Int. J. Heat Mass Transf. 115 (2017) 73–79 Dec.

[35] E. Pop, V. Varshney, A.K. Roy, Thermal properties of graphene: fundamentals and applications, MRS Bull. 37 (12) (2012) 1273–1281 Nov..

[36] Imerys, "TIMREX® C-THERM™ 002-Imerys-datasheet," Jul-2020. [Online]. Available: https://polymer-additives.specialchem.com/product/a-imerys-timrex-c-therm-002. [Accessed: 11-Apr- 2021].

[37] M. Bahrami, M.M. Yovanovich, J.R. Culham, Thermal joint resistances of non-conforming rough surfaces with gas-filled gaps, J. Thermophys. Heat Transf. 18 (3) (2004) 326–332.

[38] M. Bahrami, M.M. Yovanovich, J.R. Culham, Thermal joint resistances of conforming rough surfaces with gas-filled gaps, J. Thermophys. Heat Transf. 18 (3) (2004) 318–325 May.

[39] M.R. Conde, Properties of aqueous solutions of lithium and calcium chlorides: formulations for use in air conditioning equipment design, Int. J. Therm. Sci. 43 (4) (2004) 367–382.